

## EXTENDED EXPERIMENTAL PROCEDURES

## Mice

The R26-pCAG-nuc-3 × mKate2 knockin mouse strain was established in our laboratory. A vector harboring all of the required elements, including the CAG promoter from pPyCAG-BstXI-IP (Niwa et al., 1991), the cDNAs encoding the nuclear localization signal of the SV40 Large T-antigen (PKKKRKV) and the triplicated mKate2 from pmKate2-C (Evrogen), the woodchuck hepatitis post-transcriptional regulatory element (WPRE) from pTRIPZ (Thermo Scientific Open Biosystems), and the bovine growth hormone polyA sequence from pPyCAG-BstXI-IP, was constructed by inserting these sequences at the Sall and NotI sites of pENTR-1A (Invitrogen). In addition the Puro-resistance gene cassette (pPGK-PuroR-poly A) flanked by FRT sequences was inserted at the EcoRV site of the vector. The resulting expression vector (pENTR-1A\_CAG-nuc-3 × mKate2-WPRE-PuroR) was then mixed with the ROSA26 targeting vector (Abe et al., 2011), which contains the Reading Frame Cassette B from the Gateway Conversion System (Invitrogen) at the blunted KpnI and Ascl sites, to perform the LR recombination reaction using the Gateway system. In the resulting targeting vector, the insertion cassette was in the same orientation as the ROSA26 gene. The targeting vector was purified and introduced into HK3i C57BL/6 mouse embryonic stem (ES) cells as described previously (Kiyonari et al., 2010) with some modification, and the homologous recombined, puro-resistant ES cell clones were isolated for further culture and expansion. An aliquot of the cells was lysed and screened for successful homologous recombination by PCR. The integrity of the targeted region was confirmed by PCR using primers annealing outside the homologous recombination arms and within the inserted cassette. The primers used for the screening and the confirmation of genome integrity were as follows: 1) forward primer annealing to the region upstream of the 5' homologous arm: 5'-TGCTGGCCTACTGCTGCCTCGATCTTAC-3', 2) reverse primer annealing to the region downstream of the 5' homologous arm: 5'-AGGACAACGCCACACACCAGGTTAGC-3', 3) forward primer annealing to the region upstream of the 3' homologous arm: 5'-CGTGGTGGAGCCGTTCTGTGAGACA-3', 4) reverse primer annealing to the region downstream of the 3' homologous arm: 5'-GGTGAAATGCTTGACTCCTAGACTT-3', 5) reverse primer annealing to the CAG promoter: 5'-CAGCCAGCGGGCCATTACCGTAAGTTAT-3', and 6) forward primer annealing to the poly-A region of the puro-resistance gene: 5'-TCCATCAGAAGCTGGTCGATC-3'. The copy number of the inserted cassette was confirmed with a quantitative PCR assay using primers annealing to the coding sequences of the puro-resistance gene (forward primer: 5'-CTCGACATCGGCAAGGTGTG-3', reverse primer: 5'-GGCCTTCCATCTGTTGCTGC-3'), normalized to the amount of TATA-box binding protein gene amplification (forward primer: 5'-CCCCCTCTGCACGAAATCA-3', reverse primer: 5'-GTAGCAGCACAGAGCAAGCAA-3') (Tsuji et al., 2013) using the SYBR Premix Ex Taq GC (Takara #RR071A) and the ABI PRISM 7900 (Applied Biosystems). The selected ES cell clones were injected into 8-cell-stage ICR embryos to generate ~100% ES cell-derived chimeras (Kiyonari et al., 2010).

We also used the R26-H2B-EGFP (CDB0238K) and R26-H2B-mCherry (CDB0239K) mouse strains ([http://www.cdb.riken.jp/arg/reporter\\_mice.html](http://www.cdb.riken.jp/arg/reporter_mice.html)) (Abe et al., 2011) and the Thy1-YFP-H transgenic mouse strain (Feng et al., 2000) to observe static fluorescent gene-expression patterns in whole-brain imaging (Figure 3, S3, S5 and S7).

For the SCN immunostaining assay (Figure 4 and S4), R26-H2B-EGFP knockin mice housed under 12 h:12 hr light-dark conditions were sacrificed for fixation at ZT0 and ZT12. C57BL/6 wild-type mice or *Cry1<sup>-/-</sup>*, *Cry2<sup>-/-</sup>* mice (van der Horst et al., 1999) were adapted to light-dark conditions for over 2 weeks followed by maintenance under constant dark (DD) conditions. The sampling was performed after 24 hr of exposure (CT12 of day-0 to CT12 of day-1) to DD conditions, at CT12 and 18 of day-1, and at CT0 and 6 of day-2. Samples were obtained from multiple animals within 30 min.

To obtain fixed brains from these mice, each animal was anesthetized with an overdose of pentobarbital (>100 mg/kg, i. p.; Somnopenyl, Kyoritsu Seiyaku, Japan). The subject was transcardially perfused with PBS containing ~10 U/mL of heparin (Wako Pure Chemical Industries, Japan) to flush the blood vessels and followed by perfusion with 4% (w/v) paraformaldehyde (PFA) in PBS (pH 7.4) for fixation. The acrylamide-embedded brain sample of CLARITY protocol was prepared as described previously (Chung et al., 2013).

The Arc-dVenus transgenic mice (line D) (Eguchi and Yamaguchi, 2009) were housed under DD conditions for about 2.5 days followed by 1500 lux of white light stimulation from CT2.5. After 5 hr of the stimulation, the mice were sacrificed for fixation together with an unstimulated animal (Figure 6A). We conducted the light stimulation and sampling of multiple animals within ± 30 min. For sampling, the mice were deeply anesthetized with ether. Then, the subject was transcardially perfused with PBS containing 5 U/mL of heparin (Wako Pure Chemical Industries, Japan) to flush the blood vessels and followed by perfusion with 4% (w/v) PFA in 0.1 M PB (pH 7.4) for fixation.

Each excised brain was postfixed with the same fixation solution for 18 to 24 hr at 4°C. The fixed brain was immersed in 20% (w/v) sucrose in PBS at 4°C to remove PFA and for the following cryopreservation. If necessary, the sample was stocked in O.C.T. compound (Sakura Finetek, Japan) at -80°C until use. When the frozen sample was used for CUBIC protocol, it was thawed and washed with PBS and then immersed in CUBIC reagents. Note that the freezing step is merely for stocking samples and not compulsory.

All experimental procedures and housing conditions were approved by the Animal Care and Use Committee of the RIKEN Kobe Institute or by the Gifu University Animal Experiment Committee, and all of the animals were cared for and treated humanely in accordance with the Institutional Guidelines for Experiments using animals. All mouse strains were maintained by crossing onto a C57BL/6 background.

### Marmoset

We studied a newborn infant marmoset at the age of three days, an offspring of a breeding pair aged three and four years. The animals were housed in home cages measuring 1670 × 610 × 620 mm under 12 h:12 hr light-dark conditions (light: 08:00–20:00). Each cage had four wooden perches, a food tray, and an automatic water dispenser. Animals were fed twice a day with solid food (CMS-1, CLEA Japan, Tokyo, Japan) soaked in water, mixed with suitable amounts of powdered milk formula, honey, gluconic acid calcium, vitamin C, and lactobacillus probiotic. In addition, their diet was supplemented with chopped boiled eggs or bananas once a week. Water was provided ad libitum. For fixed brain sampling, the three-day-old marmoset was anesthetized with an overdose of pentobarbital (40 mg/kg, i.p.; Somnopentyl, Kyoritsu Seiyaku, Japan) after an intramuscular injection of ketamine (30 mg/kg; Ketalar, Daiichi Sankyo Propharma, Japan). The subject was transcardially perfused with PBS containing ~10 U/mL heparin (Wako Pure Chemical Industries, Japan) to flush the blood vessels and followed by perfusion with 4% (w/v) PFA in PBS (pH 7.4) for fixation. The excised brain was postfixed with the same solution for 18 to 24 hr at 4°C. The fixed brain was immersed in 20% (w/v) sucrose in PBS at 4°C and finally stocked in O.C.T. compound (Sakura Finetek, Japan) at –80°C until use. Animals were maintained and handled in accordance with the recommendations of the United States National Institutes of Health, and all procedures were approved by the Animal Care and Use Committee of the RIKEN Kobe Institute.

### Chemical Screening

The usage of one fixed whole brain per one chemical compound (or one chemical configuration) is not desirable for first chemical screening because it is time-consuming, labor-intensive and even unethical to prepare numbers of fixed mouse brains to test many chemical configurations. Therefore, we developed a new evaluation protocol, in which we exchanged the order of fixation and isolation, and also introduced homogenization processes (chopping and sonication) in order to test many chemical configurations using only one mouse brain. An adult mouse brain was removed from the skull, chopped with a blade, suspended and sonicated in PBS, and gradually mixed with the same volume of 8% (w/v) PFA in PBS (pH 7.4). The resulting fixed brain suspension was washed with PBS several times and finally used for the solubilization assay in Figure 1A and 1B to evaluate the clearing efficiency of each cocktail. The suspension was centrifuged to remove PBS, and resuspended in candidate chemical solutions (10 wt% in water) followed by 24 hr of incubation at room temperature. The OD600 of the incubated mixture was measured with the PowerWave XS and the attached operation software (Bio-Tek). The relative OD600s were calculated by fitting to a standard curve generated by diluting several concentrated mixtures of the suspension in PBS. The relative transmittance value of each sample (defined as 100% minus the relative OD600) was qualitatively consistent with the expected brain-clearing capability (Figure 1A, graph of the right panel). The chemical solutions were also mixed with recombinant EGFP (0.1 mg/mL, final concentration) and incubated for 12 hr at room temperature, and the resulting fluorescent signals were measured with the ARVO MX (PerkinElmer, USA). The values of the chemical solutions (without the fluorescent protein) were also measured and subtracted as the background signal. Relative fluorescence was calculated by normalization with an EGFP sample that was mixed and incubated with PBS, and titrated to show linearity. All data were calculated as an average of duplicated measurements, and two independent experiments were performed (Figure 1B and C). The chemicals were also assayed for their effects on the fluorescence of EYFP, mCherry (0.1 mg/mL, final concentration) and mKate2 (0.05 mg/mL, final concentration) in addition to EGFP in Figure 2C, but are shown as raw fluorescent values. To prepare the recombinant fluorescent proteins, the genes encoding them (containing a His-tag at the N terminus) were cloned into pET15b (Merck Millipore) and transformed into the *E. coli* BL21/DE3 strain. Overexpressed proteins were purified with Ni-NTA agarose (QIAGEN) according to the manufacturer's instructions. The refractive indices of the solutions in the chemical screening were measured by an Abbe refractometer (ATAGO, DR-A1, Japan).

We have developed improved brain tissue clearing reagents by comprehensive chemical screening described above. During the screening process, we followed the principle that brain clearing reagents should be developed that: a) minimize light scattering in the sample by adjusting the inner RI to approximately 1.5, and b) preserve the signals from fluorescent proteins and antibodies to visualize functional activities and obtain structural information. Since hydrophobic lipids are a major source of light scattering in the fixed brain, the adjustment of RIs using hydrophobic reagents has traditionally been used to transparentize the brain. The classic BABB protocol involves an initial dehydration step with ethanol followed by an RI-adjustment step with benzyl alcohol:benzyl benzoate (1:2 ratio), resulting in transparent brain specimens. However, both steps suppress EGFP fluorescence (Hama et al., 2011). Among hydrophobic organic chemicals, the use of THF as a dehydrant and DBE as an RI-adjusting medium increased the preservation of EGFP fluorescence with improved tissue transparency (Becker et al., 2012). However, EYFP fluorescence was still significantly quenched by DBE (Ertürk et al., 2012; Ke et al., 2013). Thus, it may be intrinsically difficult for hydrophobic media to provide efficient clearing with fluorescence signal preservation. In contrast, Sca/e was developed based on water-soluble clearing reagents (Hama et al., 2011). Sca/e contains kosmotropic glycerol (which stabilizes intermolecular interactions) and chaotropic urea (which disturbs hydrogen networks) as hydration-promoting agents. Since Sca/e promotes the optical clearing of brain specimens despite its relatively low RI (1.38), the chemicals in Sca/e may permeate the brain tissue efficiently. Sca/e also preserves the signals of fluorescent proteins. The original Sca/e protocol (e.g., Sca/eA2) is suitable for clearing fetal mouse brains, but has drawbacks such as a long incubation time and sample swelling (Ke et al., 2013). Another hydrophilic clearing reagent, SeeDB, a highly concentrated fructose aqueous solution that functions as an RI-adjusting medium, overcomes these issues (Ke et al., 2013). Brain specimens treated with SeeDB are transparentized within a few days, and do not show sample expansion. These features are

partly due to SeeDB's high RI and osmotic pressure, which leads to the exclusion of water molecules and the permeation of fructose molecules. However, highly myelinated adult brain samples treated with these hydrophilic reagents were not sufficiently transparent for observation using rapid whole-brain imaging with LSM. Thus, while the hydration-promoting and hydrophilic clearing reagents were effective in some cases, improvements were needed to increase their applicability. Although it may be difficult to promote dehydration with water-soluble chemicals, the simultaneous improvements in dehydration and RI homogenization by a highly osmotic and RI-aqueous medium like SeeDB was a promising approach. Based on these previous findings, we sought to develop a simple and efficient tissue-clearing protocol.

We used a comprehensive chemical screening approach to gain insight into the chemical mechanisms that contribute to effective clearing. Our improved strategy reduced the number of mice required and facilitated the quantitative evaluation of a reagent's clearing ability by measuring the transparency of a homogenized suspension instead of a whole brain. Although polyhydric alcohols including glycerol have traditionally been used, their clearing ability against hydrophobic lipids and proteins had not been quantitatively evaluated. Unexpectedly, #18 glycerol and other hydrocarbon polyols [except #11 1,4-bis(2-hydroxyethoxy)-2-butynol] did not cause a significant increase in the transparency of brain suspension in our experiment (Figure 1B). In contrast, our screening revealed that a series of aminoalcohols transparentized the suspension quite efficiently. Positively charged amino groups may contribute to the neutralization of negatively charged phospholipids, which are the most abundant lipids in the brain (Morell and Quarles, 1999). As expected, all of the tested detergents were relatively effective in clearing the suspension. Among them, the nonionic detergents (except for a specific Triton X-100) quenched the EGFP fluorescence (Figure 1C). Deoxycholate was the best candidate for clearing detergents in the first screening, but led to EGFP quenching in the presence of aminoalcohol and urea. Chaotropic agents such as urea are well-known surfactants that disrupt noncovalent interactions such as protein-protein, protein-lipid, and lipid-lipid associations. Urea has been shown to clear brain tissue effectively (Hama et al., 2011), although the chemical mechanism is poorly understood. We further investigated the clearing ability of urea-related chemicals such as aprotic solvents without amide, urea-like amides, and other chaotropic agents. Aprotic solvents without amide (#31 acetonitrile, #39 dimethylsulfoxide, and #40 1,4-dioxane) and urea-like amides (#29 *N,N*-dimethylacetamide and #30 *N,N*-dimethylformamide) did not significantly clear the suspension. Other urea-like amides (#32 oxamide, #34 *N*-carboxymethylurea, and #37 biuret) were difficult to dissolve in water. Among the chaotropic agents, #38 thiourea caused higher transparency than #36 urea, while #33 guanidine hydrochloride did not clear the suspension. Our chemical screenings in this study and the previous work on *Scale* indicated that urea's chemical structure and chaotropic ability would contribute to the efficient clearing of brain tissues. Taking into account the heterogeneity of the biochemical components in the brain, we prepared reagent 1, which consisted of aminoalcohol, Triton X-100 and urea, analogous to the components in *ScaleA2* reagents (Figure S1B). Another urea-like molecule, formamide, can be also used for tissue-clearing as indicated in the recent study (*Clear<sup>T</sup>*) (Kuwajima et al., 2013). Comparison between urea and formamide in the CUBIC protocol will be a subject of future investigation.

Reagent 1 treatment of the whole mouse brain resulted in a highly transparent sample (Figure 2A). The lipid-rich white matter was not completely cleared, however, suggesting that lipid removal was incomplete and that the RIs of the reagent and the sample were imperfectly matched. We sought to identify additional reagents that might increase brain tissue transparency through RI adjustment. As a solute's concentration increases, the osmotic pressure and RI increase simultaneously. Thus, large water-soluble molecules such as sugars are excellent candidates for solutes that will yield high-RI solutions. Fructose is one of the most water-soluble solutes, but aminoalcohols obtained from our screening would react with the aldehyde group of fructose, resulting in a brownish color via the Maillard reaction. Thus, sucrose was selected instead. Previous studies used a 60% sucrose aqueous solution for brain clearing (Tsai et al., 2009), but the clearing efficiency was much lower than for *Scale* or SeeDB (Hama et al., 2011; Ke et al., 2013). We prepared a highly osmotic, high-RI solution, reagent 2 (RI = 1.48-1.49), by mixing concentrated sucrose with cocktails based on the reagent 1 composition. When reagent-1-treated brain samples were then subjected to reagent 2, deeper regions of the brain, including the dense lipidic myelin sheath were transparentized (Figure 2A). In addition, sample swelling was minimized because the permeation of chemicals into the tissue was balanced by osmotic dehydration during reagent 2 treatment. The combination of reagent 1, *Scale*-inspired chemicals that promote tissue permeation, and reagent 2, a highly osmotic, high-RI aqueous reagent that promotes RI-homogenizing dehydration, resulted in improved clearing of the adult mouse whole brain without denaturing fluorescent proteins and antibodies.

### Measurement of Light Transmittance

Brain sample transmittance was measured with the CM-5 spectrophotometer (Konica-Minolta, Japan). For this, 100% transmittance was calibrated with a  $5 \times 10$  mm slit, and samples were placed on a  $5 \times 2$  mm slit for measurement. The blank value was measured as the transmittance of the latter slit without the dish and sample. Each value was determined as an average of duplicate measurements. The ventral-to-dorsal transmittance of the central part of the whole brain immersed in the indicated reagents was measured for Figure 2B. The central-to-lateral transmittance of the thickest part of a hemisphere placed on a plastic bottom dish without liquid was measured for Figure 1E and S1A, to make the procedure easier and avoid difficulties cementing samples to the dish. As a result, some of the measured values exceeded 100%, which we speculate is a consequence of the hemisphere acting as a convex lens because of the mismatch in RI between the air and the CUBIC samples. In this case, the values are notated as relative values (A.U.) rather than % transmittance.

### The CUBIC Protocol

ScaleCUBIC-1 (reagent 1) was prepared as a mixture of 25 wt% urea (Nacalai Tesque, 35904-45, Japan), 25 wt% *N,N,N',N'*-tetrakis(2-hydroxypropyl)ethylenediamine (Tokyo Chemical Industry CO., LTD., T0781, Japan), and 15 wt% polyethylene glycol mono-*p*-isooctylphenyl ether/Triton X-100 (Nacalai Tesque, 25987-85, Japan). Some technical tips regarding reagent 1 preparation are as follows: 1) *N,N,N',N'*-tetrakis(2-hydroxypropyl)ethylenediamine is a highly viscous liquid and can be used as an 80 wt% working solution. 2) The quality of Triton X-100 product seems critical for preserving fluorescent signals and we highly recommend the product indicated above. When the same chemical from other vendors is used, the quenching effect on recombinant fluorescent proteins should be checked. ScaleCUBIC-2 (reagent 2) was prepared as a mixture of 50 wt% sucrose (Nacalai Tesque Inc., 30403-55, Japan), 25 wt% urea, 10 wt% 2,2',2''-nitrioltriethanol (Wako Pure Chemical Industries, 145-05605, Japan), and 0.1% (v/v) Triton X-100. We referred the concentration of urea in ScaleA2 (4 M) (Hama et al., 2011), for determining its concentration in CUBIC reagents (25 wt%). Other components were added as much as possible, considering fluorescent signals and viscosity. Both reagent 1 and 2 were prepared just prior to use. When mixed, a hot stirrer should be used except during the addition of Triton X-100. Because water evaporation will make it difficult for the highly concentrated chemicals to dissolve, the weight should be monitored frequently for the addition of evaporated water during the mixing step. After confirming that all the mixed chemicals are dissolved, the reagents are cooled to room temperature, and finally Triton X-100 is added. Both CUBIC reagents should be degassed before use.

For whole-brain clearing, fixed brain samples were immersed in reagent 1 (10 g per brain) at 37°C for 3 days with gentle shaking. The solution was then exchanged, and the brain was immersed for an additional 3 to 4 days. At that point, if the white matter is not significantly cleared, further immersion with exchanged reagent 1 may be needed. The treated brain was washed with PBS several times at room temperature with gentle shaking, immersed in 20% (w/v) sucrose in PBS, degassed (required to prevent air bubbles from remaining in the ventricle), and immersed in reagent 2 (10 g per brain) for 2 to 7 days. Further immersion increased the final transparency but also caused swelling of the sample. After imaging, the sample was again washed with PBS, immersed in 20% (w/v) sucrose in PBS, and stocked in O.C.T. compound at -80°C. For nuclear staining with SYTO 16 (Life Technologies), 0.25 to 2 μM of the stain (depending on sample size) was added during reagent 1 treatment. For nuclear staining with propidium iodide (PI, Life Technologies), 10 μg/mL of the stain was added during reagent 1 treatment. After the step, additional staining was needed: sample was subjected to a freeze-thaw step followed by further incubation in 10 μg/mL of PI/PBS for 3 days at 37°C with rotation. Then, the solution was exchanged followed by staining for an additional 3 days.

### 3D Immunostaining of CUBIC Samples

A fixed brain block was treated with reagent 1 for 3 to 6 days, washed with PBS, immersed in 20% (w/v) sucrose in PBS, and frozen in O.C.T. compound at -80°C overnight. The frozen sample was then thawed, washed with PBS, and subjected to immunostaining with the primary antibodies in 750 μl of 0.1% (v/v) Triton X-100, 0.5% (w/v) bovine serum albumin, 0.01% (w/v) sodium azide in PBS for 3 days at 37°C with rotation. The stained samples were then washed with 10 ml of 0.1% (v/v) Triton X-100 in PBS several times at 37°C with rotation and then stained with the secondary antibodies in 750 μl of 0.1% (v/v) Triton X-100, 0.1% (w/v) bovine serum albumin, 0.01% (w/v) sodium azide in PBS for 3 days at 37°C with rotation. The stained samples were then washed with 10 ml of 0.1% (v/v) Triton X-100 in PBS several times at 37°C with rotation, immersed in 20% (w/v) sucrose in PBS, degassed, and immersed in reagent 2 for 24 to 36 hr. Note that longer treatment with reagent 2 may cause nonspecific signals in the void structures such as vessels and ventricles. The following antibodies were used for the staining: rabbit anti-VIP (Immunostar 20077, 1:300), goat anti-Copeptin (Santa Cruz Biotechnology sc-7812, 1:100), rabbit anti-Synapsin I (Millipore AB1543P, 1:250), donkey anti-rabbit Alexa 647 and anti-goat Alexa 546 (Life Technologies, 1:750 each). These antibodies were mixed with the sample after filtration with an Ultrafree-MC GV Centrifugal Filter (Millipore UFC30GV00). We have succeeded in the efficient 3D-IHC of all antibodies in our study. Although we have not yet encountered less effective antibodies, we could not exclude the possibility of impaired immunostaining resulting from the urea denaturation. The most important point may be that the antibodies are polyclonal. Also, peptide antibodies such as rabbit anti-VIP and goat anti-Copeptin would minimize the urea denaturation effect. On the other hand, in case of the antibodies recognizing a specific protein conformation, the urea denaturation may critically inhibit the antigen-antibody reaction. In our protocol, the fixed hypothalamus block was incubated in the antibody cocktail for 3 days at 37°C. In Figure 4C and the right panel of Figure S4C, we found that AVP immunoreactive signal was observed in the depth of at least 800 μm. Therefore, the kinetics of penetration can be conservatively estimated at ~270 μm/day at 37°C. Although VIP signal was not observed in the depth of 750 μm, the result was consistent with previous reports that VIP fibers were terminated around the subparaventricular region (Abrahamson and Moore, 2001).

### Microscopy

Whole-brain fluorescence images were acquired with light-sheet fluorescence microscopy (LSFM) (Ultramicroscope, LaVision BioTec, Germany), combined with 488 nm and 588 nm lasers (Coherent Sapphire488LP-100 and Sapphire588LP-50), a sCMOS camera (Andor Neo 5.5) and a macrozoom microscope (Olympus MVX-ZB10) with 0.63 × objective lens (Olympus MVPLA00.63X, NA = 0.15, working distance = 87 mm) (Figure S3A). The camera and the microscope were connected to a camera adaptor (Olympus MVX-TV1X), tube lens (Olympus MVX-TLU), and the Ultramicroscope filter wheel unit (LaVision BioTec, emission filters: ET525/50 and ET650/60), with adaptors (LaVision BioTec, LV AD MVX\_1 and LV AD MVX\_2). Samples were immersed in a 1:1 mixture of silicon oil TSF4300 (Momentive Performance Materials, RI = 1.498) and mineral oil (Sigma-Aldrich, RI = 1.467) during image acquisition.

Images were captured using 2 × zoom (for mouse brain) and 1 × zoom (for marmoset brain) with the MVX-ZB10. When 2 × zoom was used, the theoretical X-Y resolution of acquired image is about 4.7 μm. We prepared a customized sample holder for capturing the image of a larger marmoset hemisphere and for easier sample handling. Each plane was illuminated from both the right and left sides, and a merged image was saved. The exposure times were adjusted according to the fluorescent signal intensities of each sample. We acquired 25 whole-brain images in total (4 × single-channel whole mouse brains taken from two directions, 4 × two color-channels whole mouse brains taken from two directions, 1 × single-channel marmoset hemisphere taken from one direction) for this study.

We quantified the level of background fluorescence in CUBIC samples (Figure 3F, 3G, 3H, and 3I). For the analysis, we used images from the R26-pCAG-nuc-3 × mKate2 mouse brain. First, we masked the regions outside the brain to precisely evaluate the background fluorescence inside the brain. To this end, we constructed the 3D NIfTI-1 image file for this brain and aligned the Waxholm-Space atlas (i.e., reference brain) to the brain. We then created a binary mask using the aligned atlas and applied it to the raw TIFF images so that all pixels that are not in an annotated region (i.e., pixels that fall outside the brain) have their intensity set to zero. We used pixels with nonzero value (i.e., inside the brain) of the resulting images for the subsequent analysis. This data set includes 646 horizontal slices, numbered from 0, so we then worked on slice 322, at the center of the brain (Figure 3F, left). Our initial step was to manually determine two thresholds that separate the low-intensity signal (smaller than 8100), medium-intensity signal (between 8100 and 35000) and high-intensity signal (greater than 35000). This was obtained by extracting these regions from the raw image (left), normalizing the three resulting images and assigning each to a channel of the false-color RGB image. We color-coded these signals in blue, green and red, respectively (Figure 3F, middle). This identifies very distinct regions, and background fluorescence is in the blue region, and appears well-below the signal of interest, in the green and red regions. This is confirmed in the right panel of Figure 3F, where all pixels with an intensity below 8100 are set to black. The background is visibly removed, while the real fluorescence signal is unaffected. To obtain more reliable background fluorescence levels while avoiding edge effects, we extended this result to slices 161–483 (50% of the total data). The background fluorescence level was associated with a peak in the low-intensity region of the image histogram, shown in Figure 3G for three slices (161, 322 and 483). For example, the peak of the background fluorescence is at intensity 7,616 for slice 322. Based on these histograms and on Figure 3F, we estimated that most background pixels have an intensity no more than 5% higher than this peak intensity ( $7616 + 5\% = 7996.8$ ). We therefore used this threshold (5% higher than the background peak), and considered intensity above this threshold as signals (e.g., 50<sup>th</sup> percentile of the signal intensity corresponds the median intensity for pixels between this threshold and the maximum intensity). We repeated this analysis for other slices 161–483, and showed 95<sup>th</sup>, 80<sup>th</sup>, 65<sup>th</sup>, and 50<sup>th</sup> percentile of the signal intensity as well as the peak intensity of the background fluorescence in Figure 3H. We also calculated the ratio between each percentile of the signal intensity and the peak intensity of the background fluorescence (Figure 3I), which indicates that the fluorescence signal is significantly brighter than the background peak.

Immunostained SCN and cerebral cortex images were acquired with an inverted confocal microscope (Leica TCS SP8) with 10 × (Leica PL APO CS, NA = 0.40, working distance = 2.2 mm) or 20 × (Leica PL APO CS2, NA = 0.75, working distance = 0.68 mm) objective lenses, and with another inverted confocal microscope (Carl Zeiss LSM700) with a 10 × (Plan Aplanachromat, NA = 0.45, working distance = 2.1 mm) objective lens. To detect most of the stained signals in the unsaturated range of intensity, laser output was gradually increased according to the Z-stack acquisition.

Arc-dVenus Tg brain images in Figure S6A were captured with fluorescence stereomicroscopy using the same settings as previously described (Eguchi and Yamaguchi, 2009). Two-photon imaging was performed using an upright multiphoton microscope (Olympus FV1000, BX61WI) combined with a MaiTai DeepSee HP-OL laser (Spectra Physics) and a 25 × objective lens for Scale (Olympus, XLSLPLN25XSVMP, NA = 0.9, working distance = 8 mm) for Figure 2D and S2, or using another upright multiphoton microscope (LSM7MP, Carl Zeiss) combined with a MaiTai DeepSee laser (Spectra Physics) and a 25 × objective lens (Olympus XLPLN25XWMP, NA = 1.05, WD = 2 mm) for Figure S5B.

### Image Data Processing

All raw image data were collected in a lossless TIFF format (16-bit images for LSFM and two-photon microscopy data, and 8-bit images for confocal microscopy data). 3D-rendered images were visualized and captured with Imaris software (version 7.6.4, Bitplane). Brightness, contrast, and gamma of the 3D-rendered images were manually adjusted with the software at minimum when visualized. Confocal and two-photon 2D images as well as a projection image of Thy1-YFP-H brain (Figure S5A) were processed and visualized with Fiji (<http://fiji.sc/Fiji>). Z-projection (maximum intensity) was performed to stack 2 to 21 sequential images with the software. Brightness and contrast were manually adjusted at minimum when visualized. Gaussian filtering was performed on the image in Figure S5B.

To facilitate the dissemination of neuroinformatics tools, the Neuroimaging Informatics Technology Initiative (NIFTI) introduced the NIfTI-1 data format (.nii extension), which is now supported by most major software packages. Detailed specifications are available on the Initiative's website: <http://nifti.nimh.nih.gov/nifti-1/>. The computational analysis described below relies on this format. NIfTI-1 files were visualized using ITK-SNAP (Yushkevich et al., 2006) (Figure 7 and S7).

To generate a NIfTI-1 file from each stack of TIFF images obtained from LSFM, we first converted the images to 16-bit PNG files using *ImageMagick*. During this conversion, we also downscaled to 25% (i.e., keeping one of every four images and changing the resolution of these images from 2560 × 2160 to 640 × 540). This was necessary because of memory limitations of the current

software tools. Using the *Convert3D* tool from ITK-SNAP, each temporary stack was converted to a NIfTI-1 file, specifying the correct spacing ( $0.02064 \times 0.02064 \times 0.04$  mm, given the downscaling) and the correct orientation (which depended on the acquisition direction). Each resulting NIfTI-1 file was visualized and manually checked for size and orientation. These NIfTI-1 files were the input for the subsequent computational analysis.

The reference atlas used in our analysis was the Waxholm Space Atlas (Johnson et al., 2010). The Canon T1 image was downloaded from the website of the International Neuroinformatics Coordinating Facility: <http://software.incf.org/software/waxholm-space>, and downscaled to  $216 \times 512 \times 256$  (again for memory concerns in subsequent steps). Spacing was adjusted accordingly. To remove surrounding nonbrain tissue, this image was then multiplied by a binary mask calculated from the WHS annotation labels (using *Convert3D*), so that only labeled areas, (i.e., only brain regions), were conserved in the atlas NIfTI-1 file used for registration, as detailed below.

### The CUBIC Informatics

To facilitate analysis across samples, whole-brain images are registered and aligned to reference structures. In our analysis, we aligned images by pairs, in which one image corresponded to the structural information (obtained via nuclear staining) and the other to the signal channel. For each pair, we performed two steps: (i) registration of the structural information to a reference, and (ii) alignment of both images, i.e., applying the transformation (calculated during the registration) to both the structural image and the signal channel image (Figure 7A).

Image registration is a very active field of research, (see e.g., (Avants et al., 2011; Woods et al., 1992)). Here, we use ANTs (Advanced Normalization Tools), which has proved successful in a number of image registration tasks (Murphy et al., 2011). When aligning our composite images with each other or to the Waxholm Space Atlas, we use affine transformations only (with mutual information, 64 bins and 300000 samples as the parameters of the ANTS function). When aligning images of the same brain obtained from opposite acquisition directions, as part of the image composition process, we allowed small nonlinear transformations to overcome differences in sharpness. These nonlinear transformations were calculated in ANTs using SyN, the symmetric normalization model (Avants et al., 2008; Klein et al., 2009). The affine parameters were unchanged, and we used  $10 \times 10 \times 10$  iterations for SyN. One file was generated for each transformation. Nonlinear transformations are not compulsory: it is also possible to use affine transformations only for this step. The results shown in Figure 7 did not use SyN. Finally, alignment was performed using the *WarpImageMultiTransform* function and the computed transformations above as parameters (i.e., the affine transformation if using affine registration only, or both the affine transformation and the diffeomorphic transformation otherwise).

The overall analysis process is summarized in Figure S7A. We first aligned and combined images of the same brain acquired from opposite directions. We then aligned these composite images to an internal reference and to the Waxholm Space Atlas. Finally, we compared the signal channel images of different brains, e.g., by subtracting them [using the *fslmaths* function from FSL (Jenkinson et al., 2012)] to highlight differences in expression in specific regions (Figures 7D and 7E).

When images from two acquisition directions were available for the same brain, combining them into a single composite 3D image ensured optimal sharpness of the 3D image throughout the brain. This was motivated by the fact that, in images taken in the ventral-to-dorsal (V-D) direction, the ventral horizontal slices were sharper, while in images taken in the dorsal-to-ventral (D-V) direction, the dorsal horizontal slices were sharper, (Figure S7C). When comparing two images of the same object, the image with more edges can be considered sharper. We therefore estimated via the Sobel operator (Gonzalez and Woods, 2002) the “edge content” of each horizontal plane of the D-V and V-D 3D images of the same brain. This operation defined two unique values,  $n$  and  $m$ , such that the relative difference in “edge content” was below 10% for planes between  $n$  and  $m$ , (Figure S7D). We respectively noted  $S_i^{VD}$  and  $S_i^{DV}$ , the horizontal slice number  $i$  from the V-D image and the D-V image previously aligned to the V-D image. We could then construct the composite 3D image, one horizontal slice at a time, with the weighted sum  $S_i^{COMP} = w \times S_i^{DV} + (1 - w) \times S_i^{VD}$  and weights  $w$  defined as follows:  $w = 0$  if  $i \leq n$ ,  $w = 1$  if  $i \geq m$  and  $w = i / (m - n) + n / (n - m)$  otherwise. The resulting image was sharp throughout the brain, (Figure S7E). We implemented the operator and the weighted sum to operate on matrices containing raw intensity values. To obtain these values from the NIfTI-1 files, and then to export the results back to the NIfTI-1 format, we used the FSL functions *fsl2ascii* and *fslascii2img*, respectively.

### SUPPLEMENTAL REFERENCES

Avants, B.B., Epstein, C.L., Grossman, M., and Gee, J.C. (2008). Symmetric diffeomorphic image registration with cross-correlation: Evaluating automated labeling of elderly and neurodegenerative brain. *Med. Image Anal.* 12, 26–41.

Gonzalez, R.C., and Woods, R.E. (2002). *Digital image processing*, Second Edition (Reading, MA: Prentice Hall).

Jenkinson, M., Beckmann, C.F., Behrens, T.E., Woolrich, M.W., and Smith, S.M. (2012). *Fsl*. *Neuroimage* 62, 782–790.

Kiyonari, H., Kaneko, M., Abe, S., and Aizawa, S. (2010). Three inhibitors of FGF receptor, ERK, and GSK3 establishes germline-competent embryonic stem cells of C57BL/6N mouse strain with high efficiency and stability. *Genesis* 48, 317–327.

Klein, A., Andersson, J., Ardekani, B.A., Ashburner, J., Avants, B., Chiang, M.C., Christensen, G.E., Collins, D.L., Gee, J., Hellier, P., et al. (2009). Evaluation of 14 nonlinear deformation algorithms applied to human brain MRI registration. *Neuroimage* 46, 786–802.

- Kuwajima, T., Sitko, A.A., Bhansali, P., Jurgens, C., Guido, W., and Mason, C. (2013). *Clear<sup>T</sup>*: a detergent- and solvent-free clearing method for neuronal and non-neuronal tissue. *Development* 140, 1364–1368.
- Morell, P., and Quarles, R.H. (1999). Characteristic composition of myelin. In *Basic Neurochemistry: Molecular, Cellular and Medical Aspects* 6th edition, G.J. Siegel, B.W. Agranoff, R.W. Albers, et al., eds., (Philadelphia: Lippincott-Raven), <http://www.ncbi.nlm.nih.gov/books/NBK28221/>.
- Tsai, P.S., Kaufhold, J.P., Blinder, P., Friedman, B., Drew, P.J., Karten, H.J., Lyden, P.D., and Kleinfeld, D. (2009). Correlations of neuronal and microvascular densities in murine cortex revealed by direct counting and colocalization of nuclei and vessels. *J. Neurosci.* 29, 14553–14570.
- Tsujino, K., Narumi, R., Masumoto, K.H., Susaki, E.A., Shinohara, Y., Abe, T., Iigo, M., Wada, A., Nagano, M., Shigeyoshi, Y., and Ueda, H.R. (2013). Establishment of *TSH β* real-time monitoring system in mammalian photoperiodism. *Genes Cells* 18, 575–588.
- Woods, R.P., Cherry, S.R., and Mazziotta, J.C. (1992). Rapid automated algorithm for aligning and reslicing PET images. *J. Comput. Assist. Tomogr.* 16, 620–633.

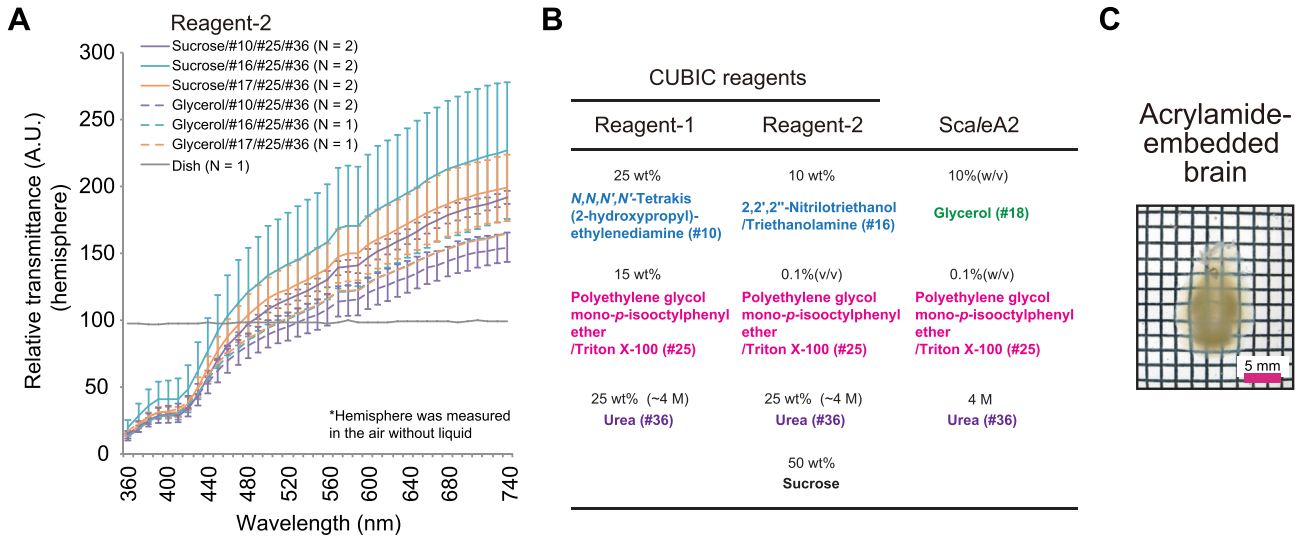


**Figure S1. Development of CUBIC Reagents by Comprehensive Chemical Screening, Related to Figure 1**

(A) Development of reagent 2, a high RI version of reagent 1. Reagent 2 candidate solutions contained 50 wt% sucrose or glycerol, 25 wt% urea, 10 wt% of an aminoalcohol and 0.1% (v/v) Triton X-100. Fixed mouse hemispheres were treated with reagent 1 (#10/#25/#36) for 5 days, washed with PBS, and immersed in each reagent 2 for 24 hr. The refractive indices of sucrose- or glycerol-containing reagent 2 were 1.48–1.49 and 1.45–1.46, respectively. After the incubation of reagent-1-treated hemispheres with the various reagent 2 candidate solutions, transmittance (360–740 nm) was measured as in Figure 1E. Sucrose-based solutions resulted in higher transmittance values than glycerol-based solutions, and 2,2',2''-nitrilotriethanol/triethanolamine (#16) tended to clear the samples more reproducibly than the other tested aminoalcohols. Note that some of the values exceeded 100 as in Figure 1E (see Extended Experimental Procedures for the details). The values represent the average  $\pm$  SEM from two independent samples. (B) Recipes of CUBIC reagents and ScaleA2. Aminoalcohols were chosen in place of glycerol. We referred to the concentration of urea (#36) in ScaleA2 (4 M) for determining its concentration in CUBIC reagents (25 wt%). However, it was calculated as wt% for ease of preparing the mixtures. Other components were added as much as possible, considering fluorescence signals and viscosity. (C) CUBIC clearing using an acrylamide-embedded brain prepared according to the CLARITY protocol. The reagent 1 and 2 were used to clear an acrylamide-embedded mouse brain (Chung et al., 2013). Although the clearing was less efficient compared to the results using “fix-only” samples (Figure 2A), the protocol could be applied to the polymer-embedded sample.

**SCALEVIEW-A2**

Thy1-YFP-H hemisphere  
treated for 3 days at 37°C

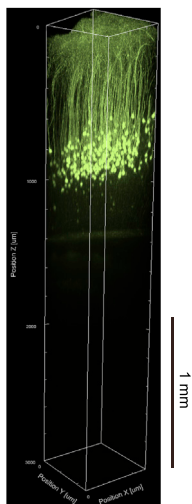


**Figure S2. Two-Photon Deep Brain Imaging of a SCALEVIEW-A2-Treated Thy1-YFP-H Tg Hemisphere, Related to Figure 2**

Two-photon deep brain imaging of Thy1-YFP-H Tg hemisphere, treated with commercially available Sca/eA2 solution (SCALEVIEW-A2 from Olympus) as in the same condition of Figure 2D (for 3 days at 37°C). The resulting sample was observed using two-photon microscopy as in Figure 2D. The performance of Sca/eA2 in a Thy1-YFP-H Tg brain after treatment for 7 days is found in the Sca/e original paper (Hama et al., 2011), and recent update of Sca/e technology will be available at <http://cfds.brain.riken.jp>.

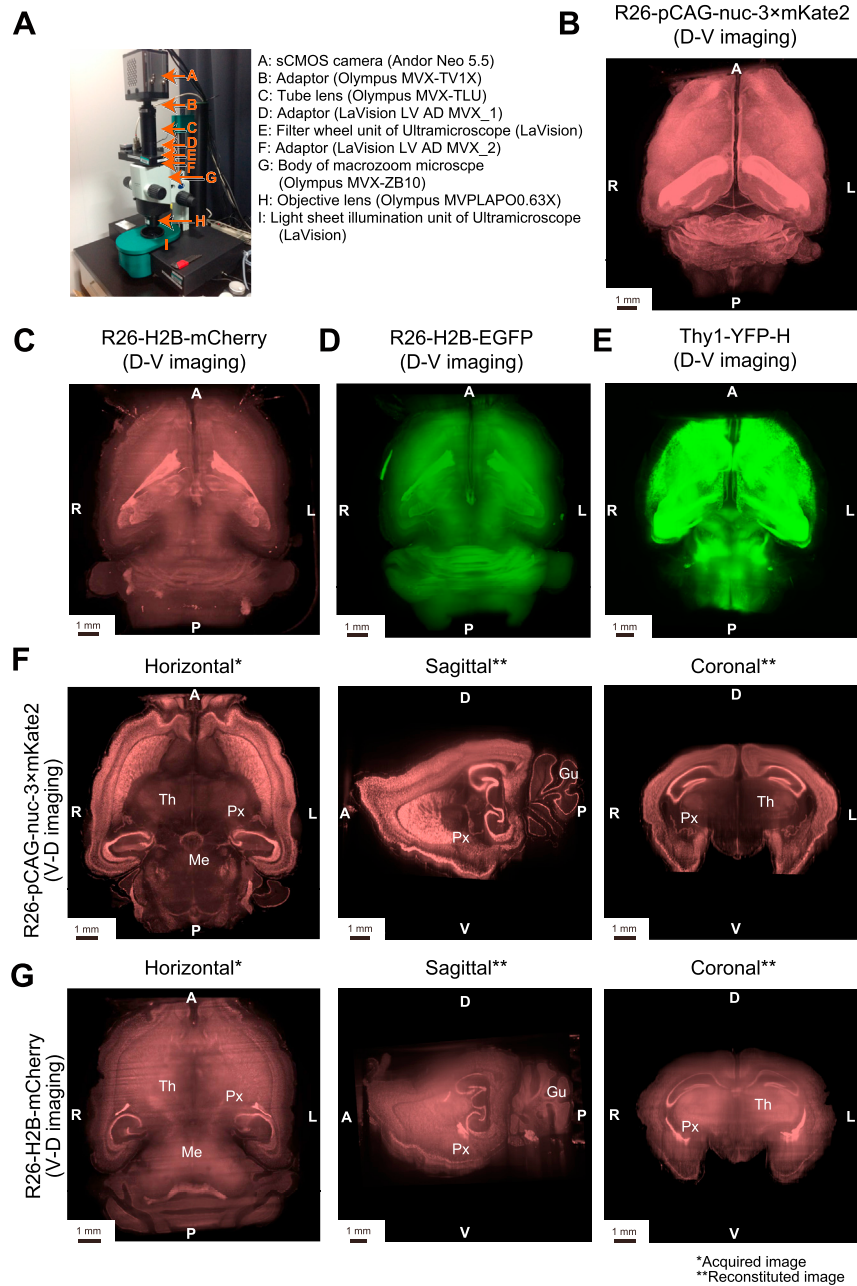


**Figure S3. Details of the CUBIC Application to Rapid Whole-Brain Imaging of Various Fluorescent Proteins, Related to Figure 3**

(A) Setup of the light-sheet fluorescent microscopy (LSFM) equipment used in this study. (B) The R26-pCAG-nuc-3 × mKate2 mouse brain (from a 5-week-old mouse) shown in Figure 3A and 3B. Images were acquired from the dorsal to ventral (D-V) direction and depicted from the ventral side in order to directly compare with Figure 3. Z-stack: 10- $\mu$ m step  $\times$  646 planes, with 0.28 s  $\times$  two illuminations. (C) D-V image of the R26-H2B-mCherry mouse brain (from a 6-month-old mouse) shown in Figure 3C. Z-stack: 10- $\mu$ m step  $\times$  696 planes, with 4 s  $\times$  two illuminations. (D) D-V image of the R26-H2B-EGFP mouse brain (from a 6-month-old mouse) shown in Figure 3D. Z-stack: 10- $\mu$ m step  $\times$  667 planes, with 4 s  $\times$  two illuminations. (E) D-V image of the Thy1-YFP-H Tg mouse brain (from a 2-month-old mouse) shown in Figure 3E. Z-stack: 10- $\mu$ m step  $\times$  733 planes, with 0.3 s  $\times$  two illuminations. (F) and (G) Selected acquired horizontal images and reconstituted sagittal and coronal images of the R26-pCAG-nuc-3 × mKate2 knockin brain (V-D imaging) and the R26-H2B-mCherry knockin brain (V-D imaging) shown in Figure 3A – 3B and 3C, respectively. Both of the genes were knocked into the same ROSA26 locus but were regulated by different promoters (the CAG promoter versus the endogenous ROSA26 promoter). The expression patterns of these proteins were compared with the corresponding reconstituted sections. Areas of differential expression are indicated. Th, thalamus; Px, ventricular choroid plexus; Me, medulla; Gu, granular layer of cerebellum. A, anterior; P, posterior; R, right; L, left; D, dorsal; V, ventral.

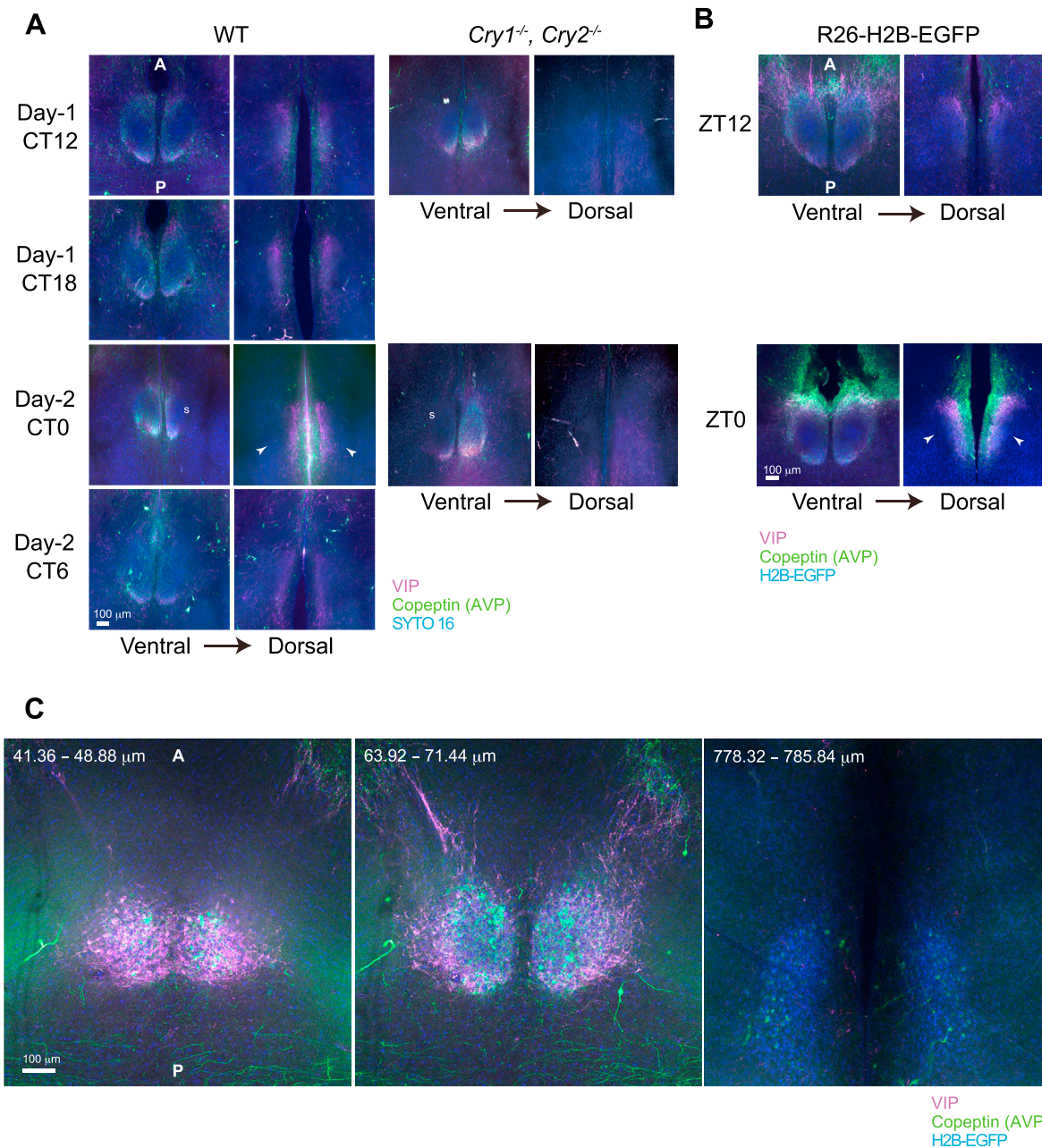


**Figure S4. Reproducibility in the Application of CUBIC to the Adult Brain Imaging of 3D Immunostained Samples, Related to Figure 4**

(A) An independent set of 3D-IHC imaging results corresponding to Figure 4D is shown. WT and *Cry1<sup>-/-</sup>, Cry2<sup>-/-</sup>* samples were stained with antibodies to VIP and Copeptin. Staining of both the WT and *Cry1<sup>-/-</sup>, Cry2<sup>-/-</sup>* SCN (day-2, CT0) was partially incomplete due to a scar in the sample (indicated as “s” in the ventral images). (B) The R26-H2B-EGFP mice housed under 12 h:12 hr light-dark conditions were sacrificed at the indicated zeitgeber time (ZT), and the fixed brains were subjected to a similar 3D-IHC analysis. Consistent with the results in Figure 4D, the dorsal fibers close to the third ventricle were more strongly stained at ZT0 than ZT12. In both panels, the depth of the horizontal images is approximately 140 μm on the ventral side and 290 μm on the dorsal side (Z-projection with maximum intensity, 1.98-μm step × 3 planes in (A) and 3.76-μm step × 2 planes in (B) from the most ventral plane of the SCN region. Strong signals of the neuropeptides detected in the dorsal side of SCN at CT0/ZT0 are indicated with arrowheads. (C) Enlarged 3D-IHC analysis images of the other R26-H2B-EGFP mice SCN (left and middle panels) and PVN (right panel), sacrificed at the ZT12 (Z-projection with maximum intensity, 3.76-μm step × 2 planes). Images were acquired and processed in a similar but an optimized condition for each sample so that most of the stained signals were obtained in the unsaturated range of intensity.

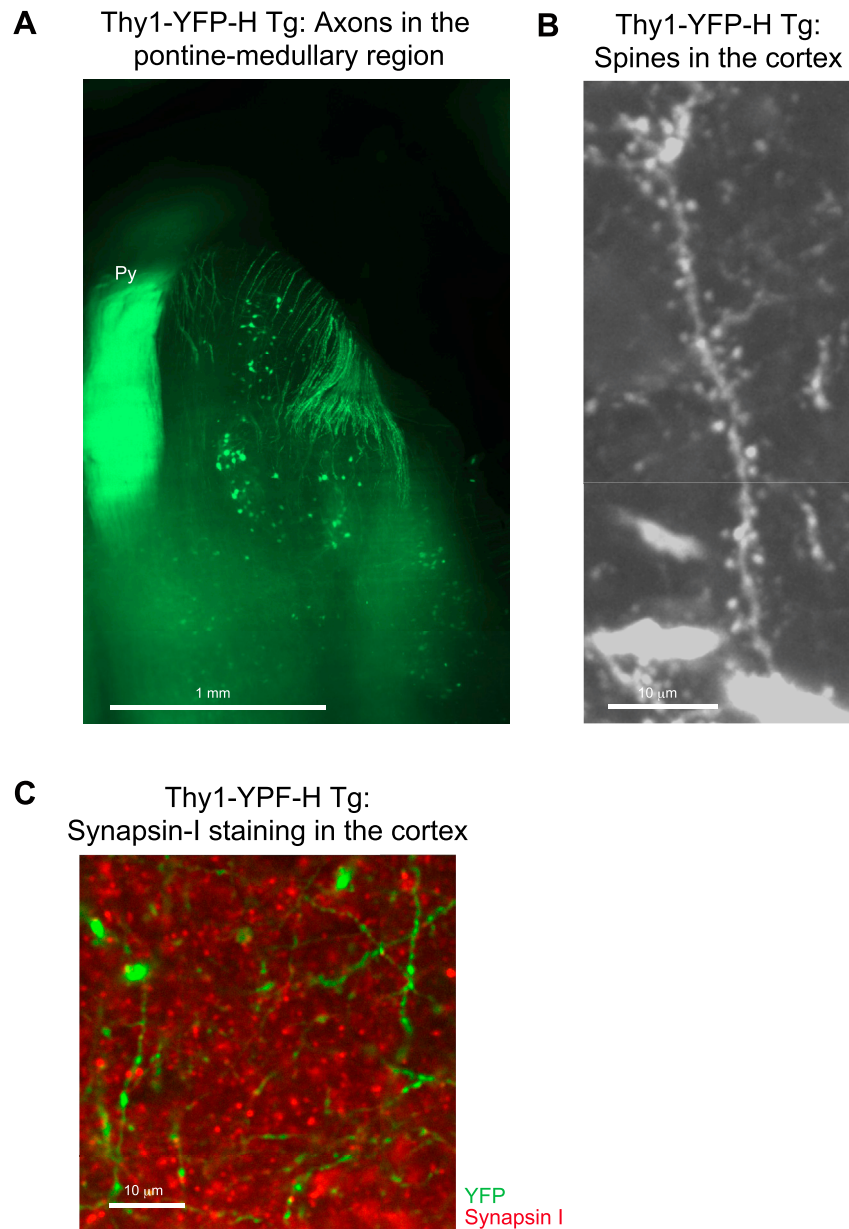


**Figure S5. CUBIC Is Scalable in Its Application to Subcellular Structure Imaging, Related to Figure 5**

(A) Axons in the pontine-medullary region of the Thy1-YFP-H Tg CUBIC brain sample, observed with LSFM. The image is a part of the Z-projection image of the V-D YFP channel imaging data shown in Figure S7B (Z-projection with maximum intensity, 10- $\mu$ m step  $\times$  21 planes). Py, pyramidal tract. (B) Spines in the cerebral cortex of the Thy1-YFP-H Tg CUBIC brain sample, observed with two-photon microscopy. The image is part of the Z-projection image of two-photon imaging data (Z-projection with maximum intensity, 0.5- $\mu$ m step  $\times$  20 planes). (C) Immunostaining with a Synapsin-I antibody in the cerebral cortex of the Thy1-YFP-H Tg CUBIC brain sample, observed with confocal microscopy. Part of an original acquired image is shown.

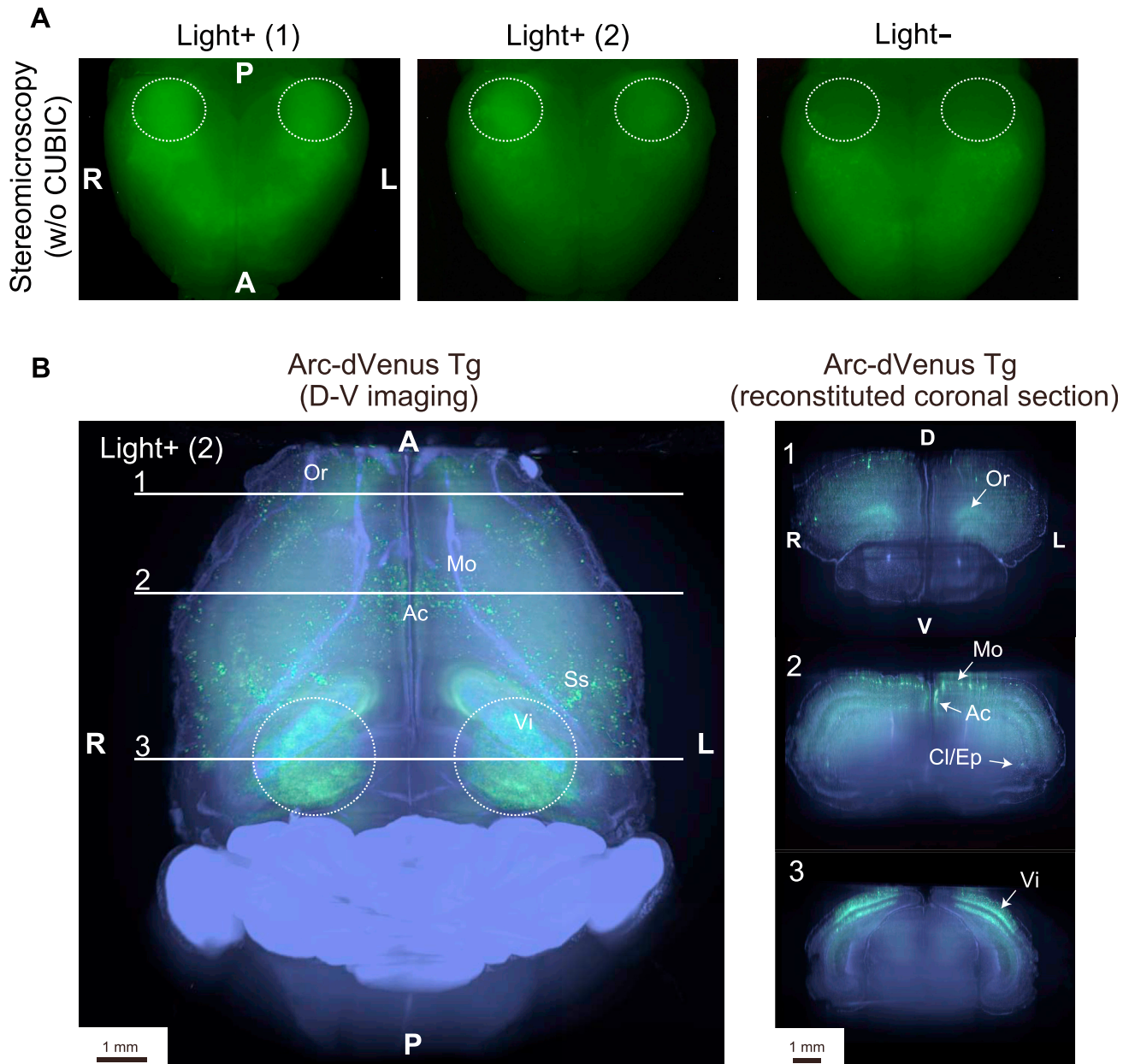


**Figure S6. Whole-Brain Nuclear Counterstaining in CUBIC Enables the Visualization of Neural Activities Induced by Environmental Stimulation, Related to Figure 6**

(A) Venus signals (green) of Arc-dVenus Tg mouse brains, which were used for Figure 6 and S6B, were also observed with fluorescent stereomicroscopy. A region including the visual area in the cortex is indicated by a dotted ellipse, encompassing the area where the Venus signals appeared in Light+ brains. (B) The Light+ (2) Arc-dVenus Tg mouse brain was subjected to CUBIC treatment, and two-color D-V images were acquired with LSFM (Z-stack: 10- $\mu$ m step  $\times$  633 planes) as in Figure 6B. Increased fluorescent signals were observed in the same regions as observed in the Light+ (1) brain shown in Figure 6B.

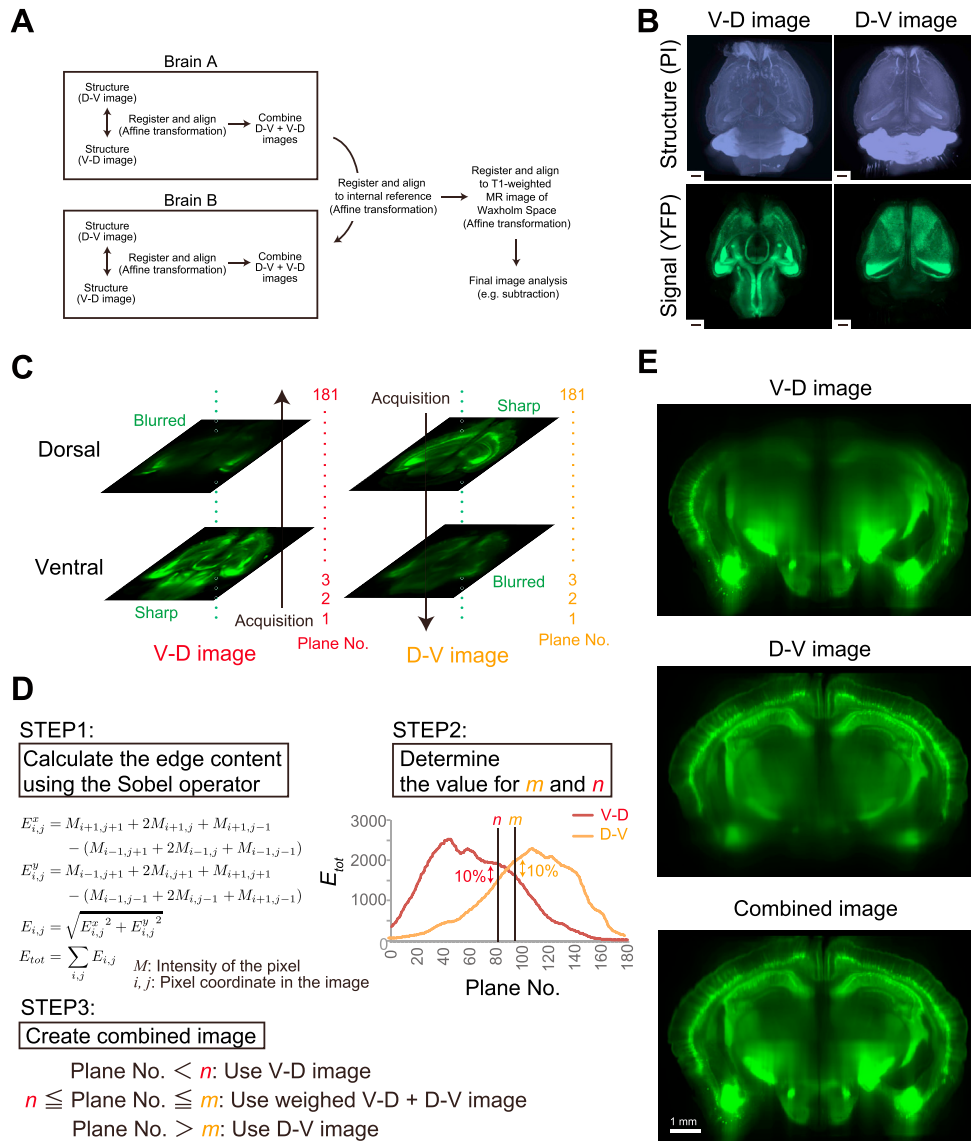


**Figure S7. Computational Image Analysis in CUBIC Enables Gene Expression Profiling of Adult Whole Brains, Related to Figure 7**

(A) Overview of computational analysis steps. For each brain, we first combined imaging data acquired in the ventral-to-dorsal (V-D) and dorsal-to-ventral (D-V) directions. To do so, we first aligned the D-V and the V-D brain images and then considered the sharpness of each horizontal plane to generate a single clear 3D image as in (C)–(E). These samples were then aligned to an internal reference brain, and to a reference atlas. This was achieved by registering the image containing structural information, and then applying the corresponding transformation to both the structural and the signal image of the same brain. Finally, the aligned signal images were compared and contrasted using methods such as subtraction, to highlight differences between samples. (B) A data set consisting of reconstituted 3D images acquired from a single Thy1-YFP-H Tg mouse brain subjected to whole-brain nuclear counterstaining with PI is shown. Structural information obtained by PI staining was used to calculate the transformation matrix. Z-stack: 10- $\mu$ m step  $\times$  722 planes for V-D imaging and 10- $\mu$ m step  $\times$  797 planes for D-V imaging, with 0.6 s  $\times$  two illuminations for YFP and with 0.15 s  $\times$  two illuminations for PI, respectively. Scale bar: 1 mm. (C) Image sharpness depended on acquisition directions. The raw data in (B) were converted to a NIFTI-1 file for further analysis. We downsampled original image data to 25% (i.e., keeping one of every four images and changing the resolution of these images from 2560  $\times$  2160 to 640  $\times$  540). During conversion, the same plane number was assigned to equivalent planes of both images. In this case, the ventral horizontal planes were sharper in the V-D image, while dorsal horizontal planes were sharper in the D-V image. The images obtained in two directions were combined to obtain a single clear 3D image. (D) Estimating the edge content to combine the two acquisition directions. A classic edge detection method is to use the Sobel operator (noted  $E_{i,j}$  here), which corresponds to a gradient estimation at pixel  $(i, j)$  of an image. Summing this value over all pixels of the image gives us the edge content  $E_{tot}$  of the image. Plotting  $E_{tot}$  as a function of the plane number, for the V-D and D-V images, confirms the observation from (C). If we note these values  $E_{VD}$  and  $E_{DV}$ , respectively, we can define a unique range  $[n, m]$  where  $|E_{VD} - E_{DV}| / E_{VD} < 0.1$ . Finally, the values for  $n$  and  $m$  are used to design a weighted sum of the V-D and D-V images (see [Extended Experimental Procedures](#)). (E) Combining the compensated V-D and D-V images from a single Thy1-YFP-H brain (NIFTI-1 file).  $n = 87$ ,  $m = 93$ .